Electronic Supplementary Material (ESI) for ChemComm.

Electronic supporting information

Supramolecular Traps for Highly Phosphorylated Inositol Sources of Phosphorus

Subhamay Pramanik,[a] Victor W. Day [a] and Kristin Bowman-James*[a]

[a]Department of Chemistry, University of Kansas, Lawrence, Kansas 66045, USA

Email: kbjames@ku.edu

Table of Contents

Section	Content	Page No.
S1	Materials and Instrumentation	S3
S2	Synthesis and Characterization	S3
S3	Crystallization Procedures	S11
S4	NMR and Mass Spectral Analyses	S12
S5	DOSY Analysis	S15
S6	X-ray Crystallographic Studies	S18
S7	References	S22

S1 Materials and Instrumentation

S1.1 Materials

All reagents, chemicals and deuterated solvents were purchased from commercial suppliers and used as received without further purification.

S1.2 Instrumentation

All NMR spectra were recorded at 298K using DMSO-d_6 and D_2O as solvents. Solution pH was measured by a Fischer Accumet pH meter. ^{1}H NMR spectra were recorded on Bruker AVIIIHD 400 MHz, Avance AVIII 500 MHz and Avance 800 MHz NMR spectrometers; ^{13}C NMR and two-dimensional NMR data were recorded on an Avance AVIII 500 MHz (125 MHz) NMR spectrometer; ^{31}P NMR spectra were recorded on Bruker 500 MHz (202 MHz) and Bruker AVIIIHD 400 MHz (162 MHz) NMR spectrometers. All ^{31}P NMR (proton decoupled) spectra were referenced by absolute referencing with their corresponding ^{1}H NMR. DOSY NMRs were recorded at Bruker Avance AVIII 600 MHz NMR. All NMR data were analyzed using MestreLab Mnova software. HREIMS$^+$ were recorded in Waters Micromass LCT Premier spectrometer.

S2 Synthesis and Characterization

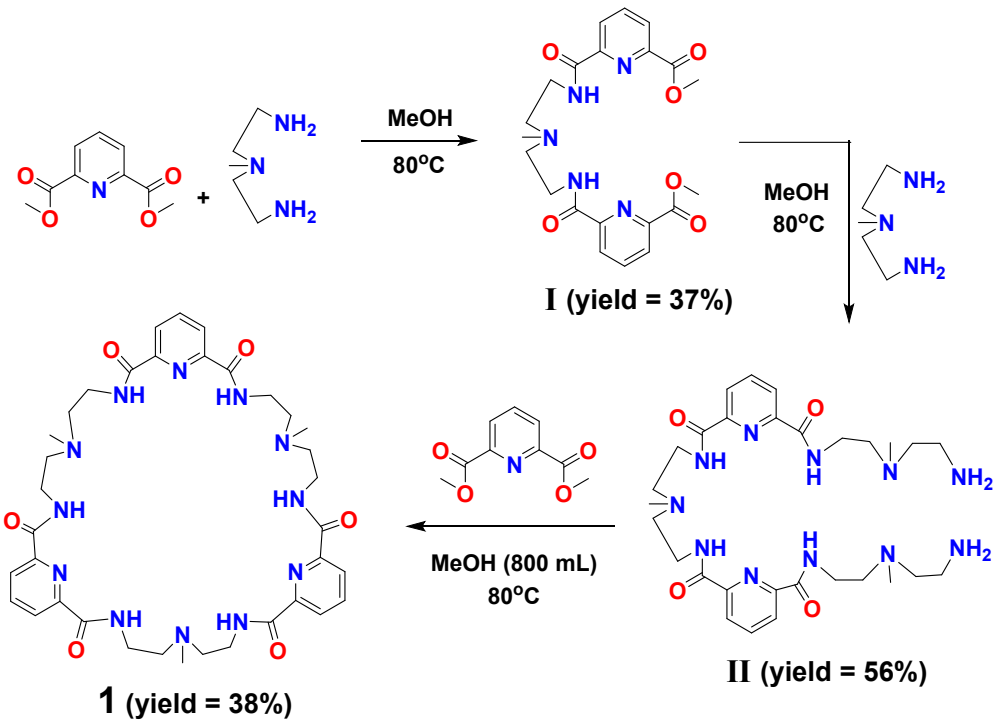

Scheme S1. Synthesis of 36-membered macrocyclic host **1**.

S2.1 Synthesis and characterization of Precursor I

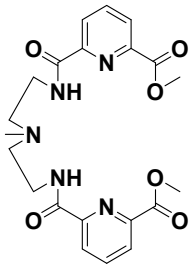

A 50 mL CH_3OH solution of N-methyl-2,2'-diaminodiethylamine (3.52 g, 30 mmol) was added dropwise (through a dropping funnel within 2 h) to a hot CH_3OH solution (100 mL) of dimethyl 2,6-pyridinedicarboxylate (23.5 g, 120 mmol). After addition, the reaction mixture was allowed to reflux for 72 h. Afterward the reaction mixture was concentrated under reduced pressure to 50 mL and cooled to room temperature. Precipitated excess dimethyl 2,6-pyridinedicarboxylate was filtered off and the filtrate was concentrated *in vacuo* and subjected to column chromatography on silica (230-400 mesh, gradient elution 3% v. CH_3OH in CH_2Cl_2 to 5% v. CH_3OH in CH_2Cl_2) to give precursor I as a white crystalline solid. Yield: 5 g (37%); ^{1}H NMR (500 MHz, DMSO-d_6) δ_H = 8.53 (t, J = 7.5 Hz, 2H, CO*NH*), 8.18-8.16 (m, 2H, Ar), 8.14-8.13 (m, 4H, Ar), 3.88 (s, 6H, OCH_3), 3.47 (q, J = 6.7 Hz, 4H, NHCH_2), 2.63 (t, J = 5.0 Hz, 4H, NHCH$_2CH_2$), 2.33 (s, 3H, NCH_3). ^{13}C NMR (125 MHz, DMSO-d_6) δ_C = 164.90, 163.41, 150.58, 146.67, 139.71, 127.46, 125.39, 56.19, 53.09, 42.47, 37.33. HREIMS+ for $[C_{21}H_{25}N_5O_6+H]^+$ calcd 444.1878, found 444.1952 $[C_{21}H_{25}N_5O_6+H]^+$ and 466.1714 $[C_{21}H_{25}N_5O_6+Na]^+$.

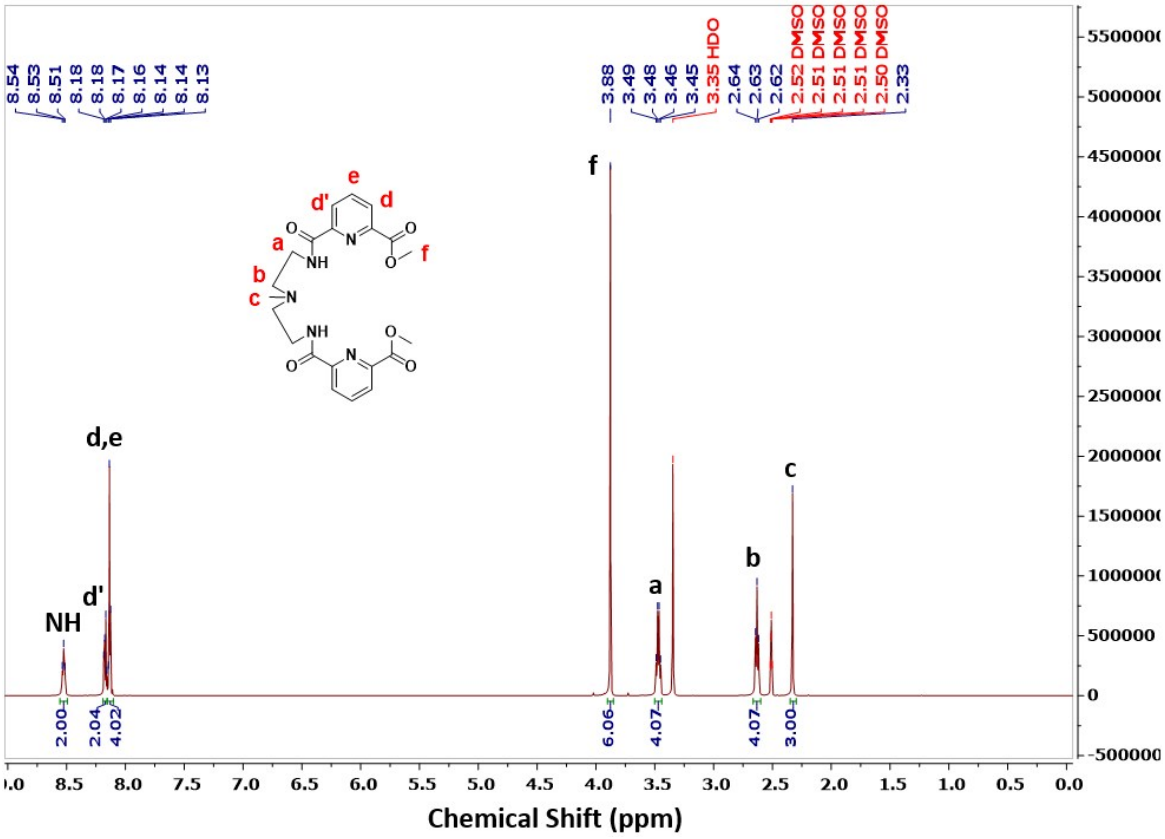

Fig. S1. ^{1}H NMR (500 MHz, DMSO-d_6) of precursor **I**.

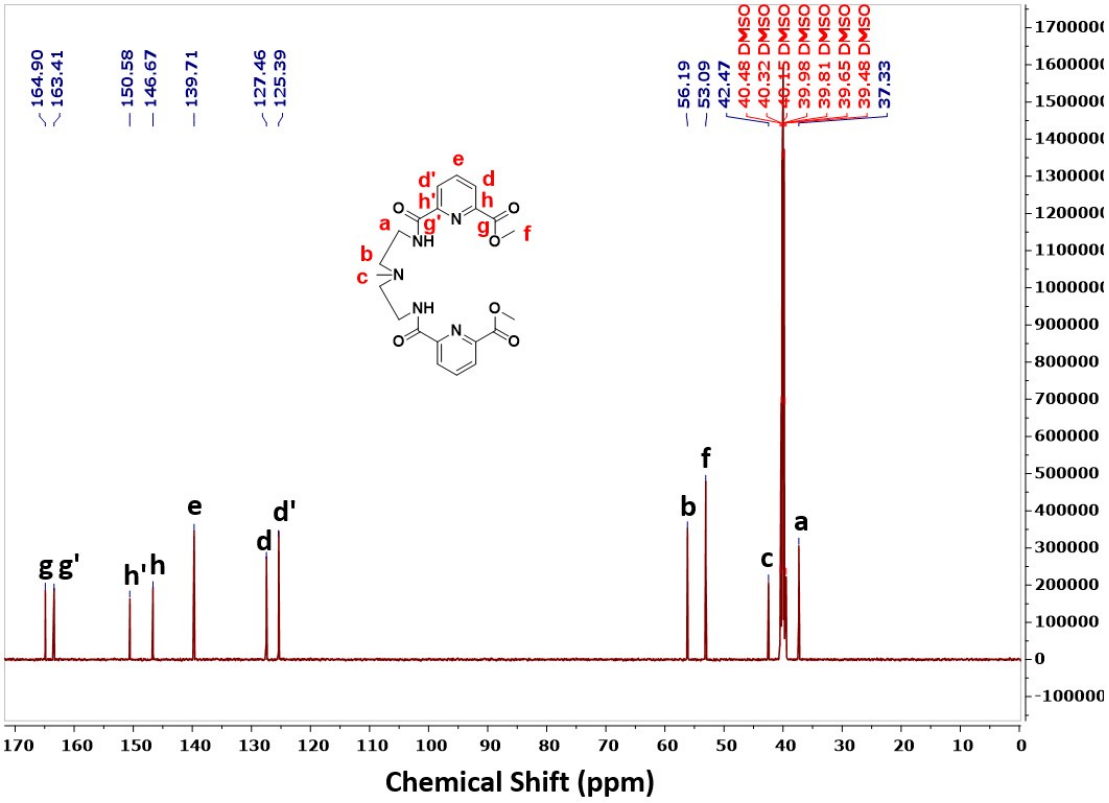

Fig. S2. ^{13}C NMR (125 MHz, DMSO-d_6) of precursor-**I**.

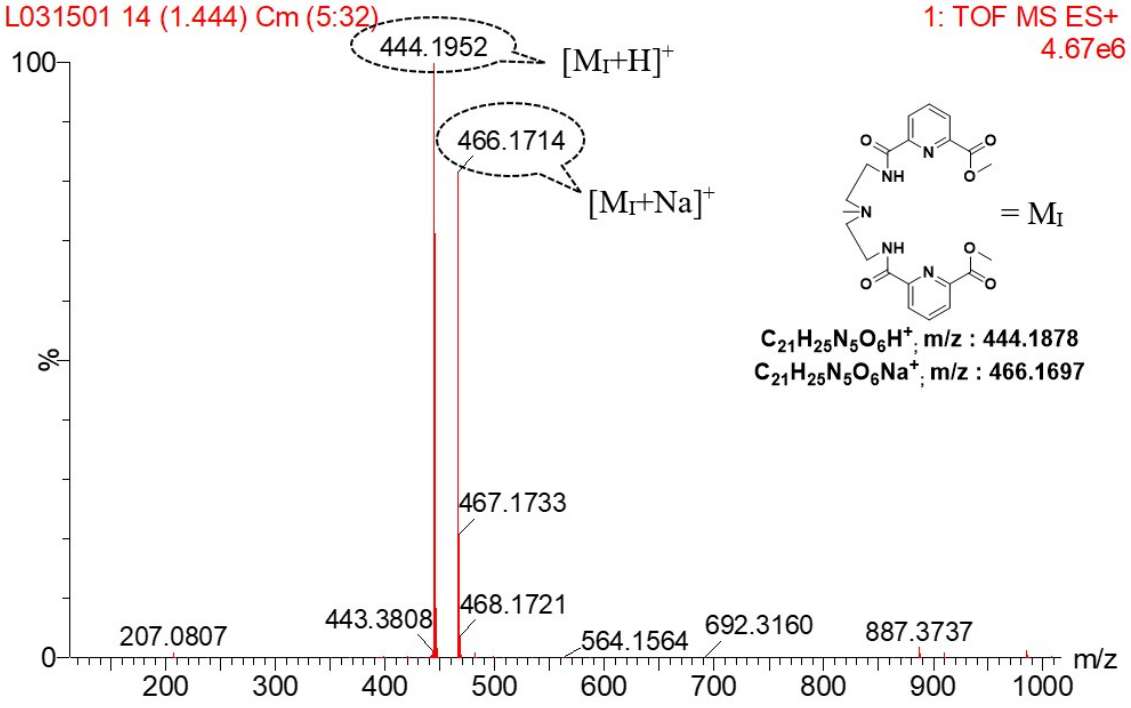

Fig. S3. ESI-MS spectrum of precursor-**I**.

S2.2 Synthesis and characterization of Precursor II

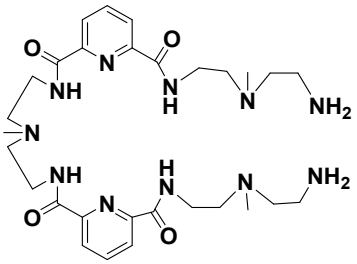

Precursor **II**

Precursor **I** (1.56 g, 3.5 mmol) was dissolved in 30 mL CH_3OH and added dropwise (through a dropping funnel over 2 h) to a 20 mL methanol solution of N-methyl-2,2'-diaminodiethylamine (2.46 g, 21 mmol) while heating in 3-necked round bottom flask (RBF). After addition, the reaction mixture was allowed to reflux for 72 h. Afterward the reaction mixture was concentrated to remove the solvent and then distilled under reduced pressure. The brown residue was subjected to column chromatography on neutral alumina (150 mesh) using 5% v. CH_3OH in CH_2Cl_2 to 10% v. CH_3OH in CH_2Cl_2 as gradient eluent to furnish precursor **II** as a dense yellow oil. Yield: 1.2 g (56%); ^{1}H NMR (500 MHz, DMSO-d_6) δ_H = 9.26 (t, J = 5.0 Hz, 2H, CO*NH*), 9.21 (t, J = 7.5 Hz, 2H, CO*NH'*), 8.18-8.12 (m, 6H, Ar), 3.47 (dq, J = 19.8, 6.4 Hz, 8H, NH*CH*$_2$ and NH'*CH*$_2$), 2.64 (t, J = 7.5 Hz, 4H, NHCH$_2$*CH*$_2$), 2.58 (t, J = 7.5 Hz, 4H, NH$_2$CH$_2$*CH*$_2$), 2.53 (t, J = 7.5 Hz, 4H, NH'CH$_2$*CH*$_2$), 2.37 (d, J = 5.0 Hz, 2H, NH$_2$*CH*$_2$), 2.35 (s, 3H, N*CH*$_3$), 2.29 (t, J = 5.0 Hz, 2H, NH$_2$*CH*$_2$), 2.22 (s, 3H, N*CH*$_3$), 2.13 (s, 3H, N*CH*$_3$). ^{13}C NMR (125 MHz, DMSO-d_6) δ_C = 163.60, 163.50, 149.16, 139.86, 124.56, 61.12, 61.00, 56.93, 56.88, 42.77, 42.73, 39.49, 37.63, 37.59. HREIMS+ for $[C_{29}H_{47}N_{11}O_4+H]^+$ calcd 614.3885, found 614.3840.

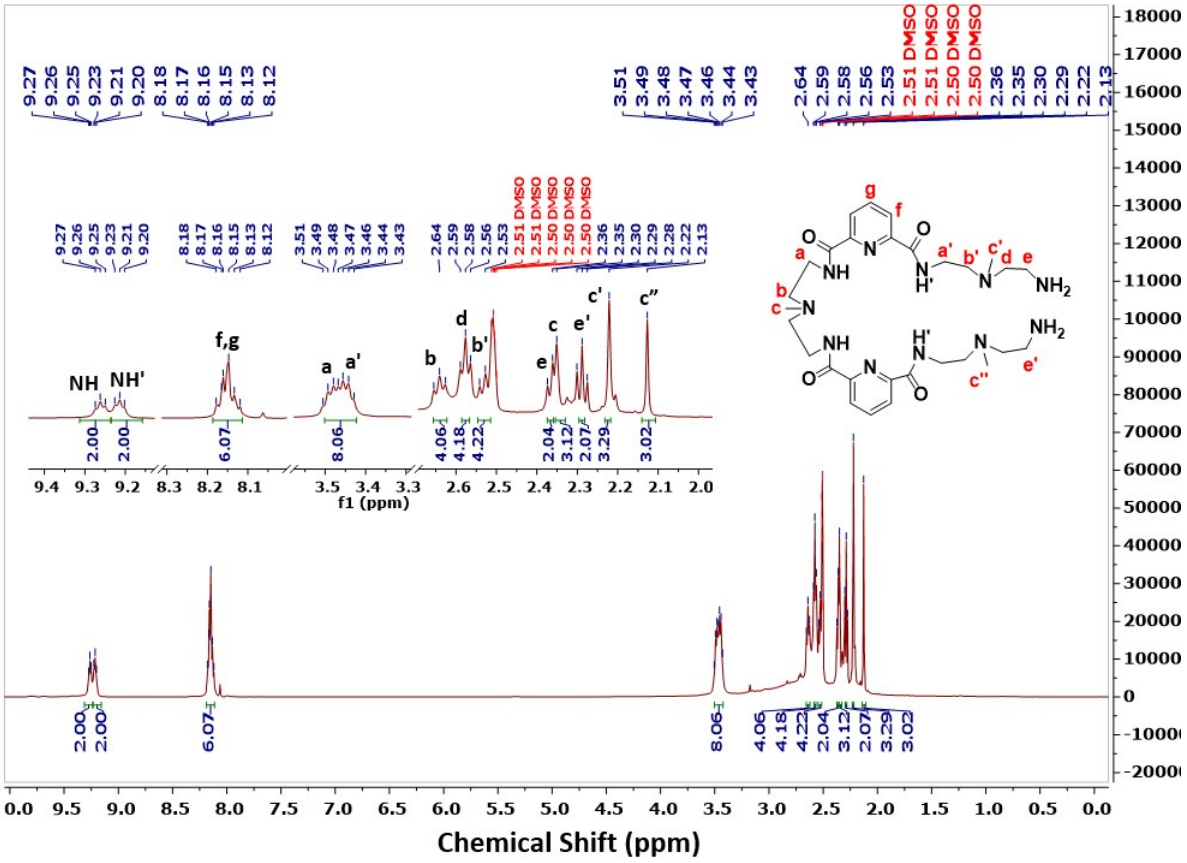

Fig. S4. Full and expanded (inset) ^{1}H NMR (500 MHz, DMSO-d_6) of precursor-**II**.

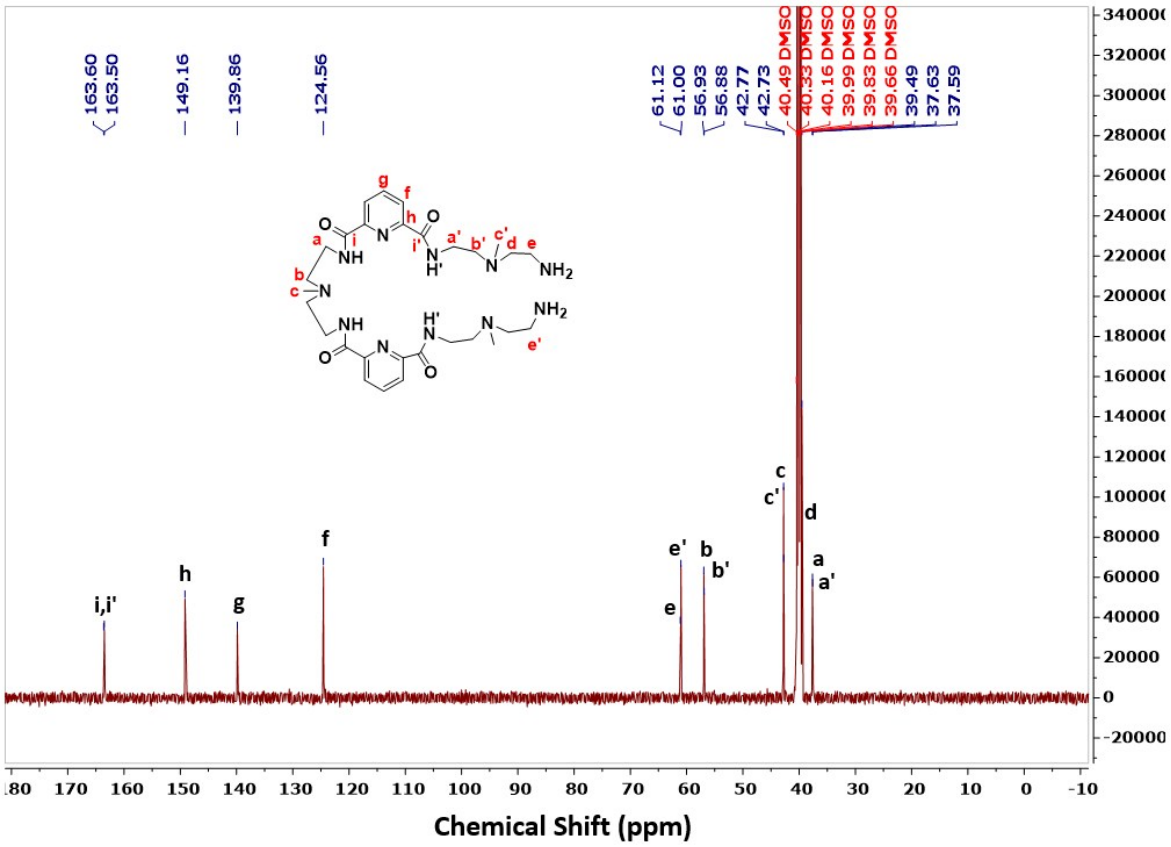

Fig. S5. ^{13}C NMR (125 MHz, DMSO-d_6) of precursor-**II**.

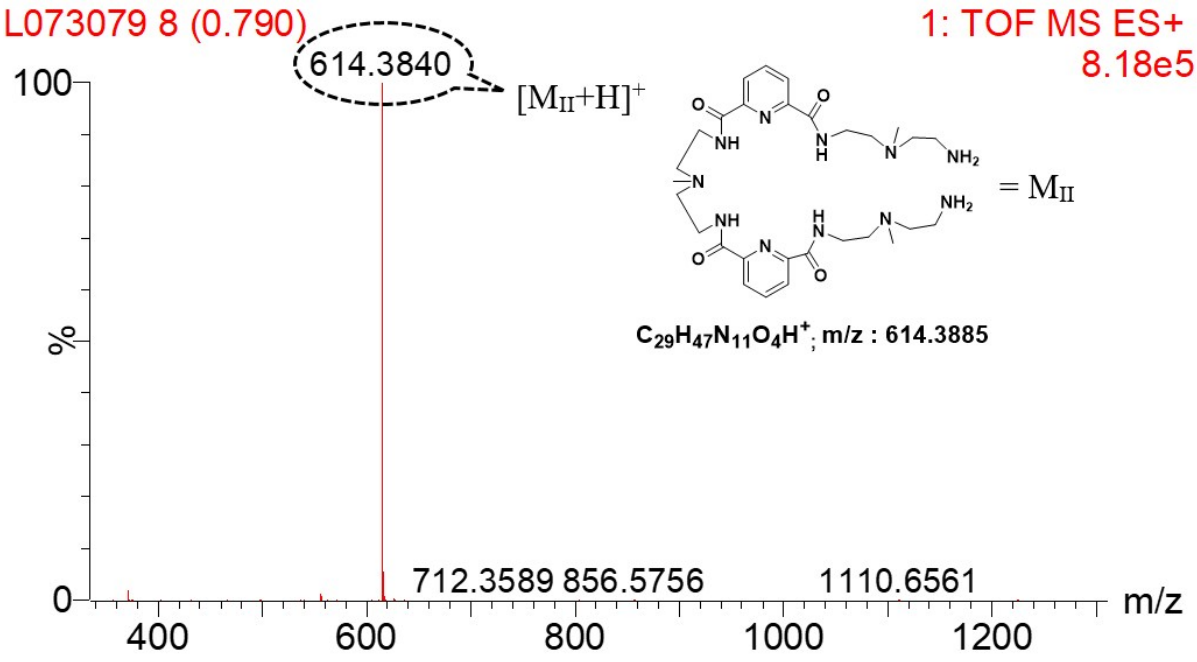

Fig. S6. ESI-MS spectrum of precursor-**II**.

S2.3 Synthesis and characterization of Macrocycle 1

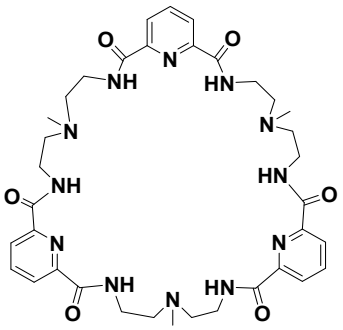

Macrocycle **1**

Precursor **II** (2.14 g, 3.5 mmol) and dimethyl 2,6 pyridinedicarboxylate (0.68 g, 3.5 mmol) were mixed in a 1000 mL RBF and dissolved in 800 mL CH_3OH followed by refluxing at 80˚C for 7 d. The reaction was monitored by spotting in precoated silica gel plates. After reactants were consumed, the reaction mixture was concentrated under reduced pressure and subjected to column chromatography on silica (28-200 mesh) using 10% v. CH_3OH in CH_2Cl_2 to 20% v. CH_3OH in CH_2Cl_2 as gradient eluent to produce a white solid which was further recrystallized with CH_3OH /CH_3CN to afford macrocycle **1** as a white solid. Yield: 1.0 g (38%); ^{1}H NMR (500 MHz, DMSO-d_6) δ_H = 9.16 (t, J = 5.0 Hz, 6H, CO*NH*), 8.14-8.09 (m, 9H, Ar), 3.45 (q, J = 6.7 Hz, 12H, NH*CH*$_2$), 2.59 (t, J = 5.0 Hz, 12H, NHCH$_2$*CH*$_2$), 2.29 (s, 9H, N*CH*$_3$). ^{13}C NMR (125 MHz, DMSO-d_6) δ_C = 163.45, 149.07, 139.84, 124.52, 56.87, 42.46, 37.50. HREIMS+ for $[C_{36}H_{48}N_{12}O_6+H]^+$ calcd 745.3893, found 745.3870.

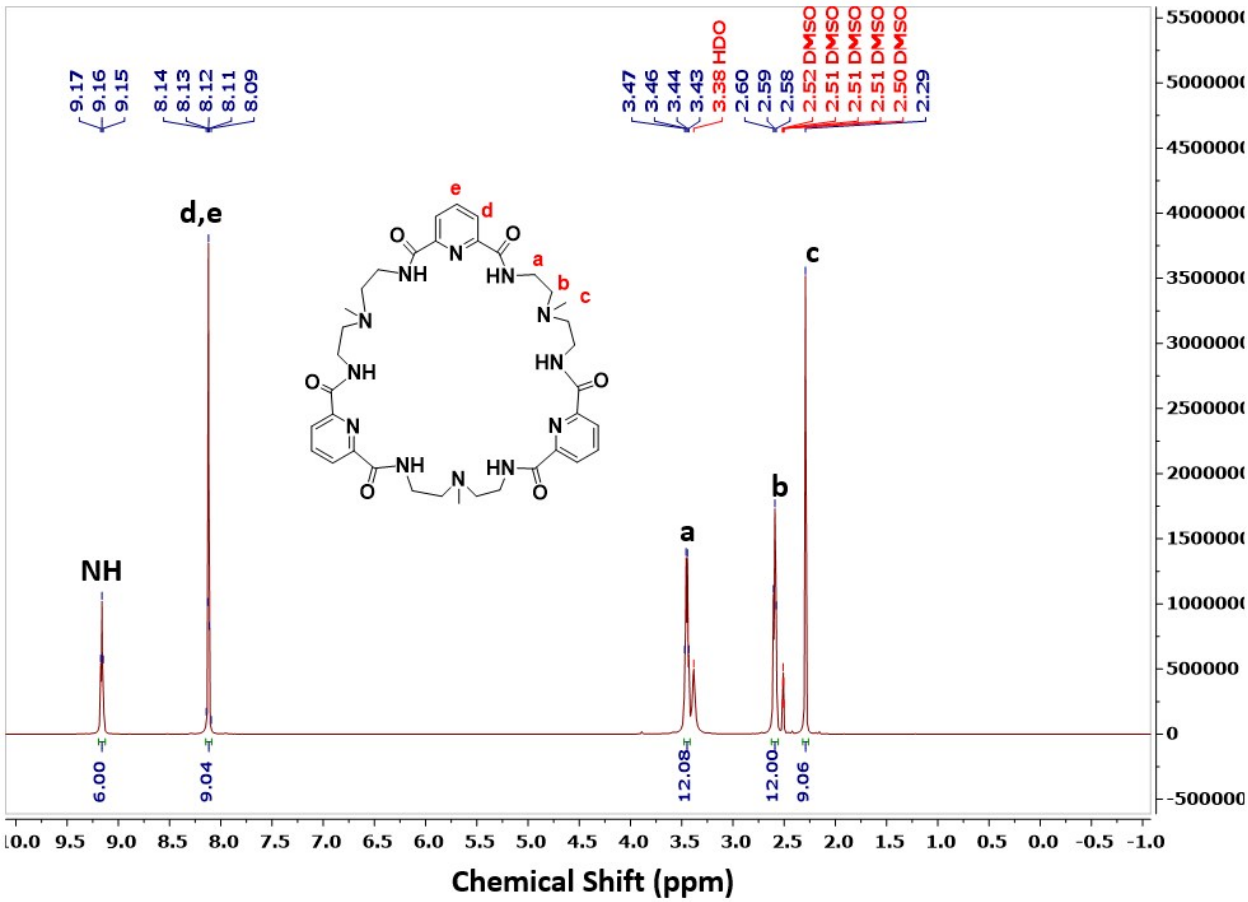

Fig. S7. Full ^{1}H NMR (500 MHz, DMSO-d_6) of macrocycle **1**.

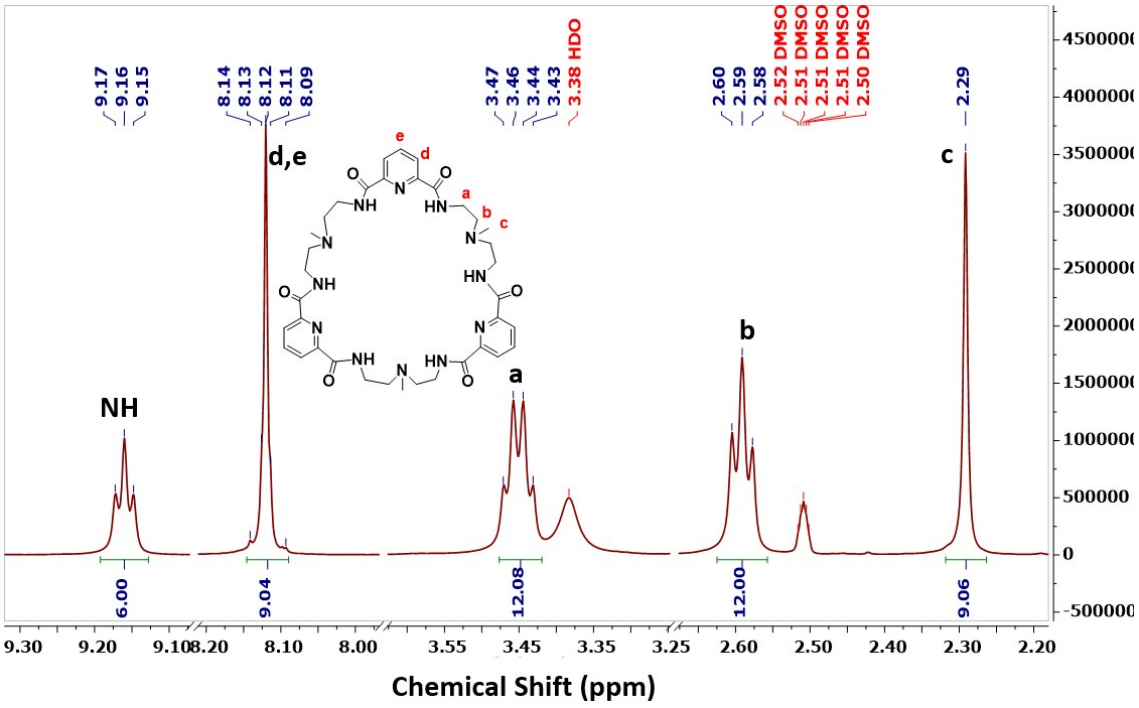

Fig. S8. Expanded ^{1}H NMR (500 MHz, DMSO-d_6) of macrocycle **1**.

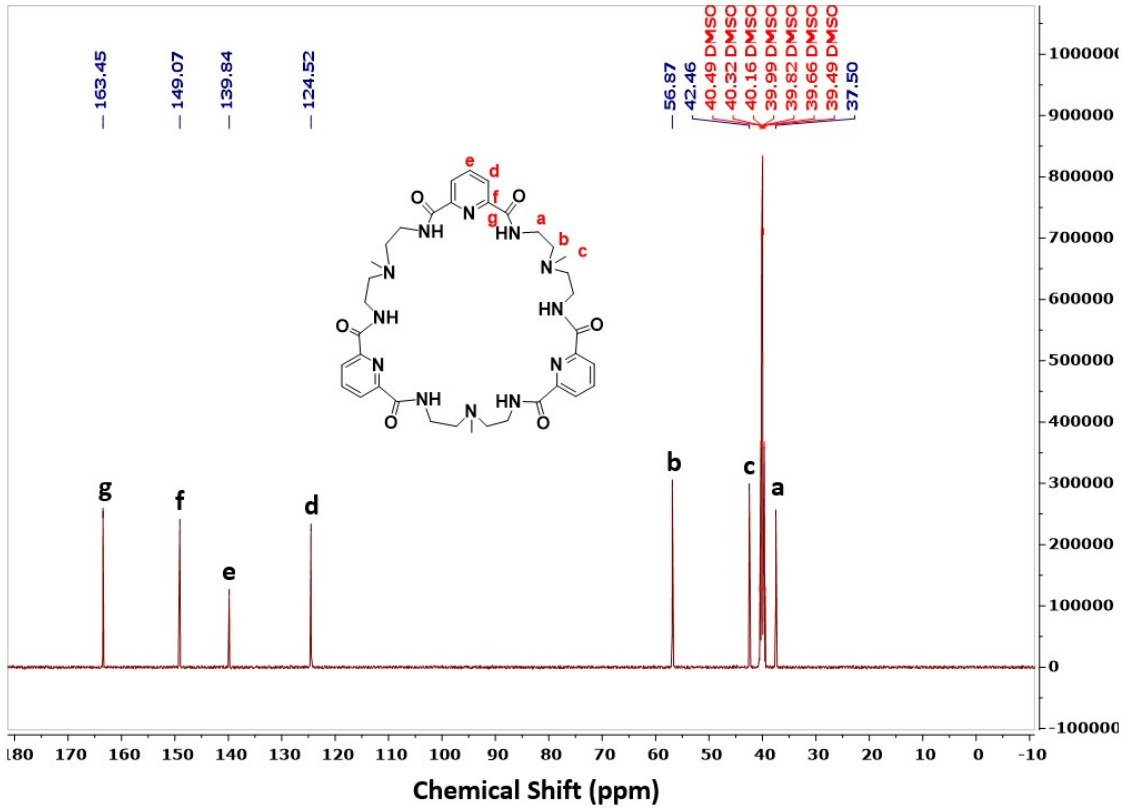

Fig. S9. ^{13}C NMR (125 MHz, DMSO-d_6) of macrocycle **1**.

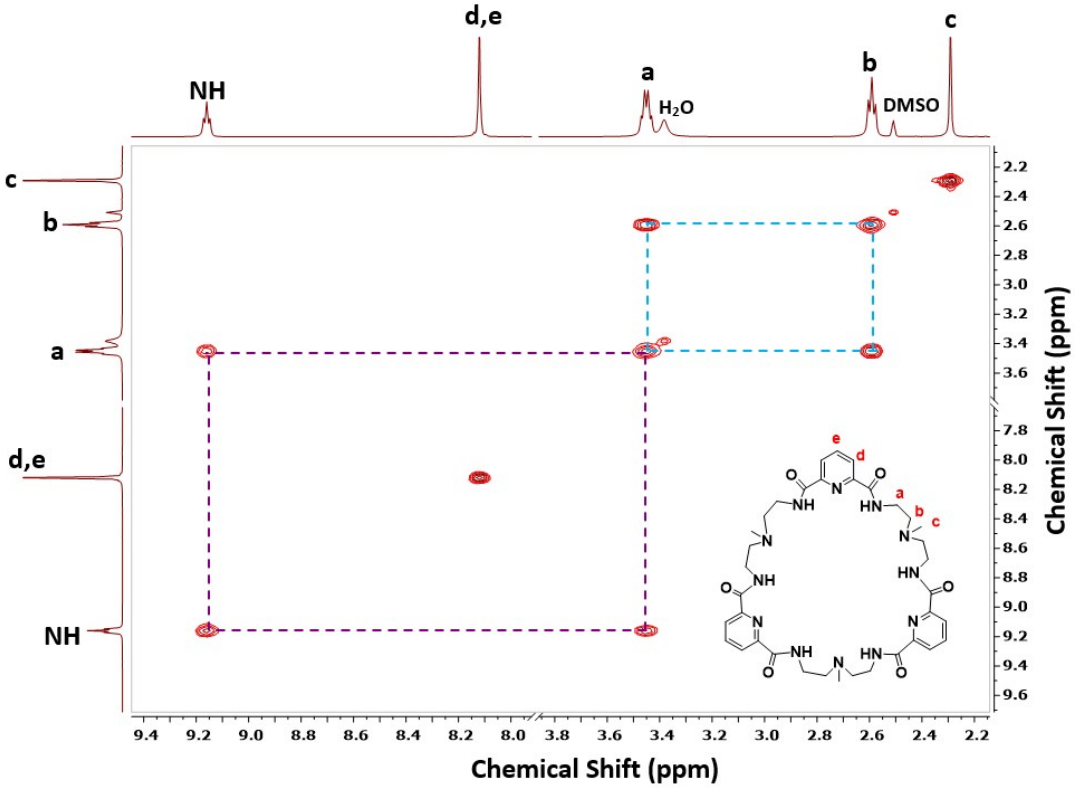

Fig. S10. ^{1}H-^{1}H COSY NMR (500 MHz, DMSO-d_6) of macrocycle **1**.

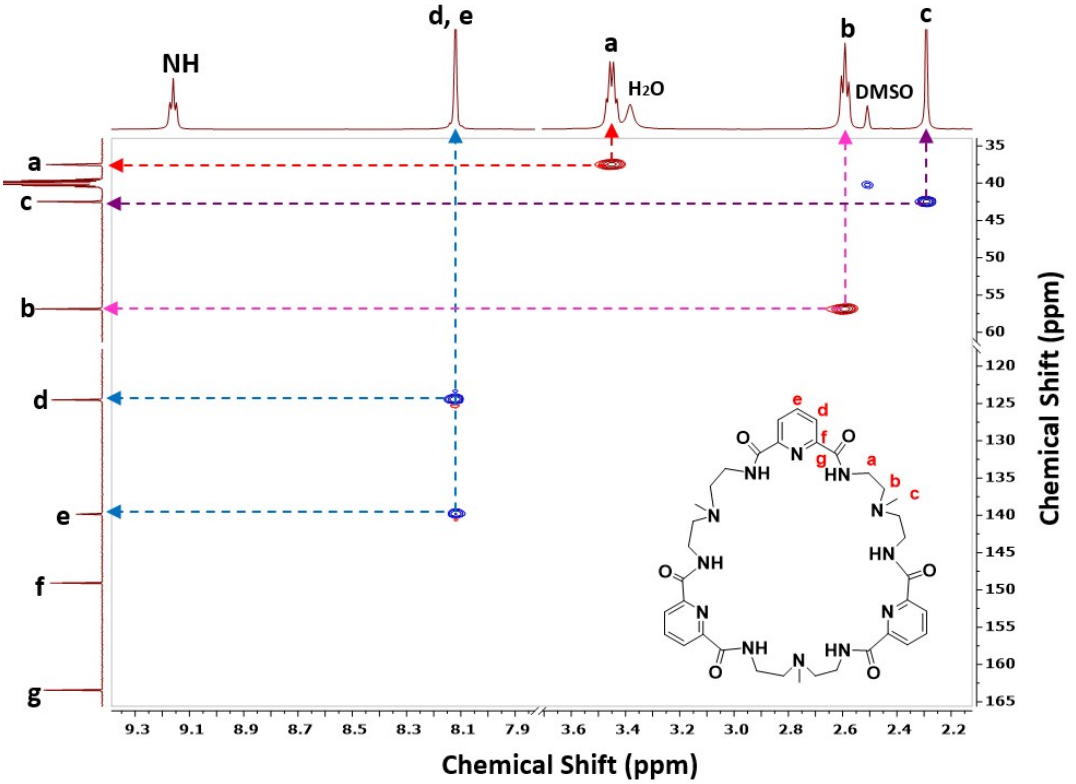

Fig. S11. ^{1}H-^{13}C HSQC NMR (500 MHz, DMSO-d_6) of macrocycle **1**.

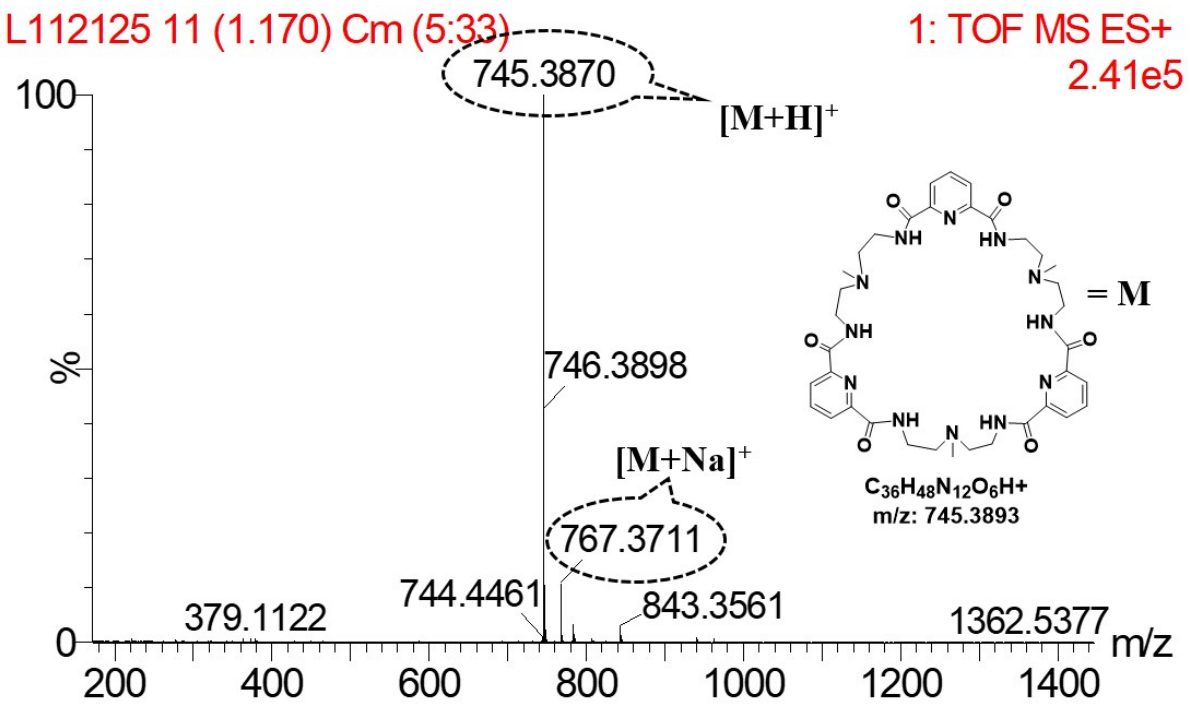

Fig. S12. ESI-MS spectrum of macrocycle **1**.

S3 Crystallization Procedures

S3.1 Crystallization of macrocycle 1

Macrocycle **1** (14.88 mg) was added to a 1 mL DMSO-d_6:D_2O (1:1) mixture (pH = 8.12) followed by sonication under mild heating to dissolve completely. The solution was set up for slow evaporation at room temperature, and very nice triclinic shaped single crystals of **1**·4H_2O were grown overnight (CCDC No: 1947225) (Fig. S18).

S3.2 Crystallization of complexes of 2 [$(H_3\mathbf{1}^{3+})_2$(*myo*-$H_6IP_6^{6-}$)] and 3 [$(H_3\mathbf{1}^{3+})_2$(*scyllo*-$H_6IP_6^{6-}$)]

A solution of the dipotassium salt, $[K^+]_2[H_{10}IP_6^{2-}]$ (8.1 mg, 1.1 equiv.), in 1 mL H_2O was added to a 1 mL CH_3OH solution of macrocycle **1** (14.89 mg, 2.0 equiv.), followed by addition of 0.5 mL DMSO and 0.5 mL CH_3CN. The resulting solution (pH = 6.26) was filtered and allowed to sit for slow evaporation at room temperature. After several months, crystals of two different morphologies were obtained that were suitable for X-ray crystallography: long monoclinic (*C2/c*) crystals of **2**·36.6H_2O·CH_3OH (CCDC No: 1947224) and parallelepiped-shaped rhombohedral ($R\bar{3}/S_6$) crystals of **3**·25.7H_2O·2CH_3CN (CCDC No: 1947283).

S4 NMR and Mass Spectral Analyses

S4.1 NMR analysis of the $[K^+]_2$[*myo*-$H_{10}IP_6^{2-}$] reagent with *scyllo*-contaminant

The ^{1}H NMR of commercially available $[K^+]_2[H_{10}IP_6^{2-}]$ from Sigma-Aldrich shows the appearance of three major peaks along with minor signals corresponding to other stereoisomers and inorganic phosphate. The signal attributed to the *scyllo* isomer showed approximately 3% upon integration (Fig. S13).
At pH 1.68, $[K^+]_2$[*myo*-$H_{10}IP_6^{2-}$] and $[K^+]_2$[*scyllo*-$H_{10}IP_6^{2-}$] exist in 1a5e and 6e conformation, respectively. Coupling constants were about 2.3-2.5 Hz for axial/equatorial proton couplings [$^3J(H_{ax}\text{-}H_{eq})$]; 9.3-9.8 Hz for both diaxial [$^3J(H_{ax}\text{-}H_{ax})$] and [$^3J$(H-P)] couplings. For the *myo*-IP_6 isomer, proton signals included: a doublet of triplets (dt) at 4.99 ppm for the equatorial H2; a triplet of doublets (td) at 4.40 ppm for the axial H1/H3; quartets (q) at 4.57 and 4.38 ppm for H4/H6 and H5 respectively, as described previously[10]. An additional tiny signal at 4.22 ppm was thought to be attributed to the *scyllo*-IP_6 isomer. It appears as a quartet due to coupling of each axial proton with adjacent axial protons and the corresponding phosphorus atom (Fig. S13). Upon ^{31}P decoupling, the signal of *scyllo*-IP_6 changes from quartet (q) to triplet (t) (Fig. S14).

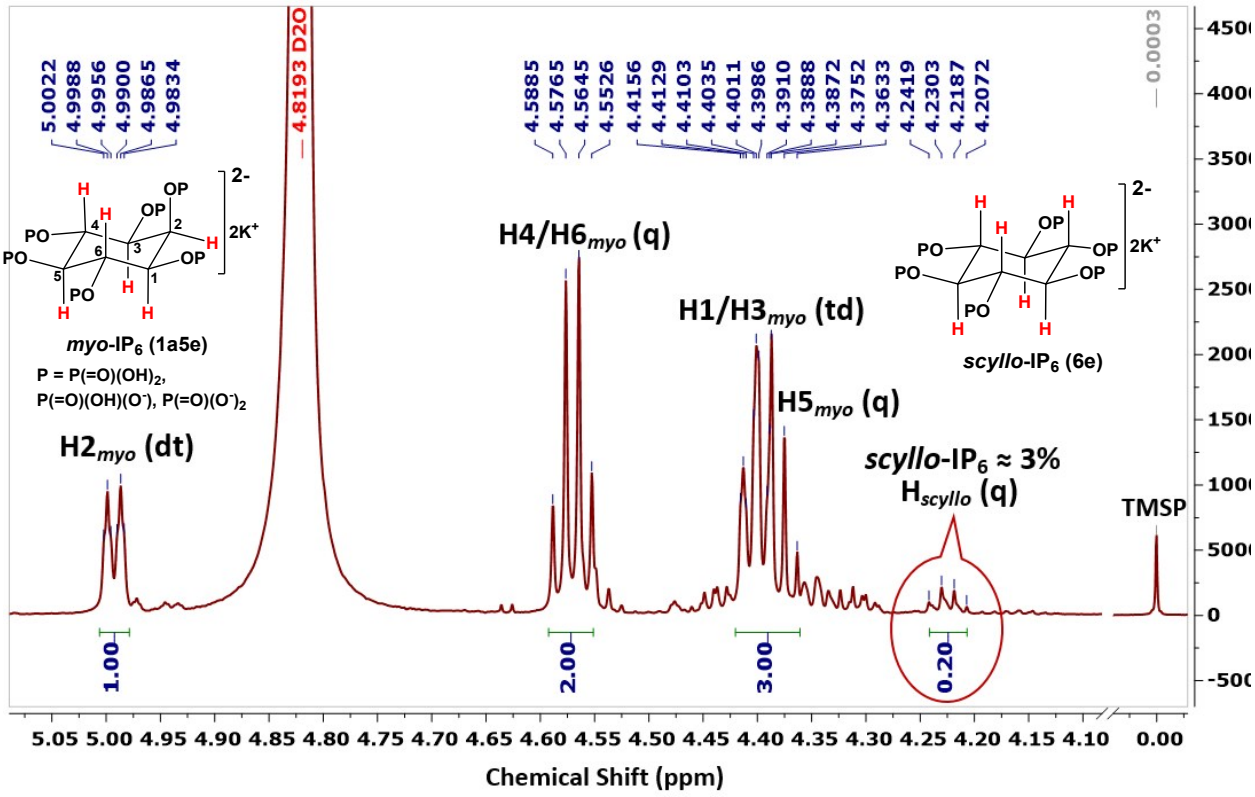

Fig. S13. Integrated ^{1}H NMR (^{31}P-coupled, Bruker Avance 800 MHz NMR) of $[K^+]_2$[*myo*-$H_{10}IP_6^{2-}$] in D_2O (pH=1.68).

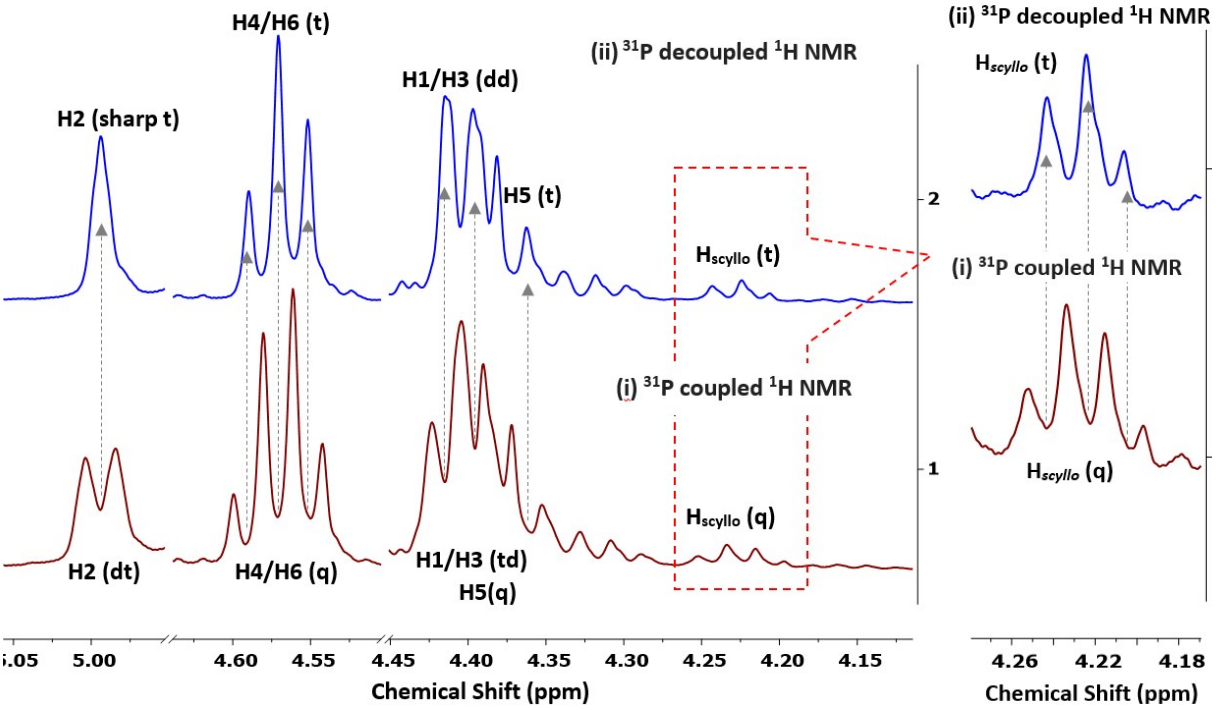

Fig. S14. ^{31}P coupled and decoupled ^{1}H NMR of the sample in D_2O (500 MHz) showing the change in multiplicity of the signals.

S4.2 NMR analysis of solution interactions of IP_6 with macrocycle 1

Solutions of macrocycle **1** (1 mL, 10 mM) and $[K^+]_2[H_{10}IP_6^{2-}]$ (0.5 mL, 20 mM) were prepared separately in two screw-cap vials in DMSO-d_6:D_2O (1:1). The ^{1}H NMR titration of the macrocycle **1** was recorded upon quantitative addition of $[K^+]_2[H_{10}IP_6^{2-}]$ in aliquots consisting of different molar ratios from **1**:IP_6, 2:0.1 to 2:2, along with measurement of pH (Fig. 4A) at each addition. Binding constants (1:IP_6 = 2:1 where $K_{1:1}$ = 3.35×10^3 M^{-1} and $K_{2:1}$ >> 10^5 M^{-1}) were calculated from the resulting titration data using EQNMR[20] and experimental error is < 5% (see Fig. 4A and B). A similar titration was carried out for the ^{31}P titration, except that a solution of the phytate was titrated with a solution of the macrocycles **1**.

S4.3 ESI-MS spectrum of phytate encapsulated macrocyclic complex

The ESI-MS (+ve ion mode) spectrum of redissolved crystals shows two major peaks at m/z 2149.5347 and 2171.6123 Dalton (Da) corresponding to $[(H_3\mathbf{1}^{3+})_2(H_6IP_6^{6-})+H]^+$ and $[(H_3\mathbf{1}^{3+})_2(H_6IP_6^{6-})+Na]^+$ species, respectively. Both experimental peaks correlate very well with their calculated mass (Fig. S15). These results clearly support that one $H_6IP_6^{6-}$ ion is trapped within two macrocycles.

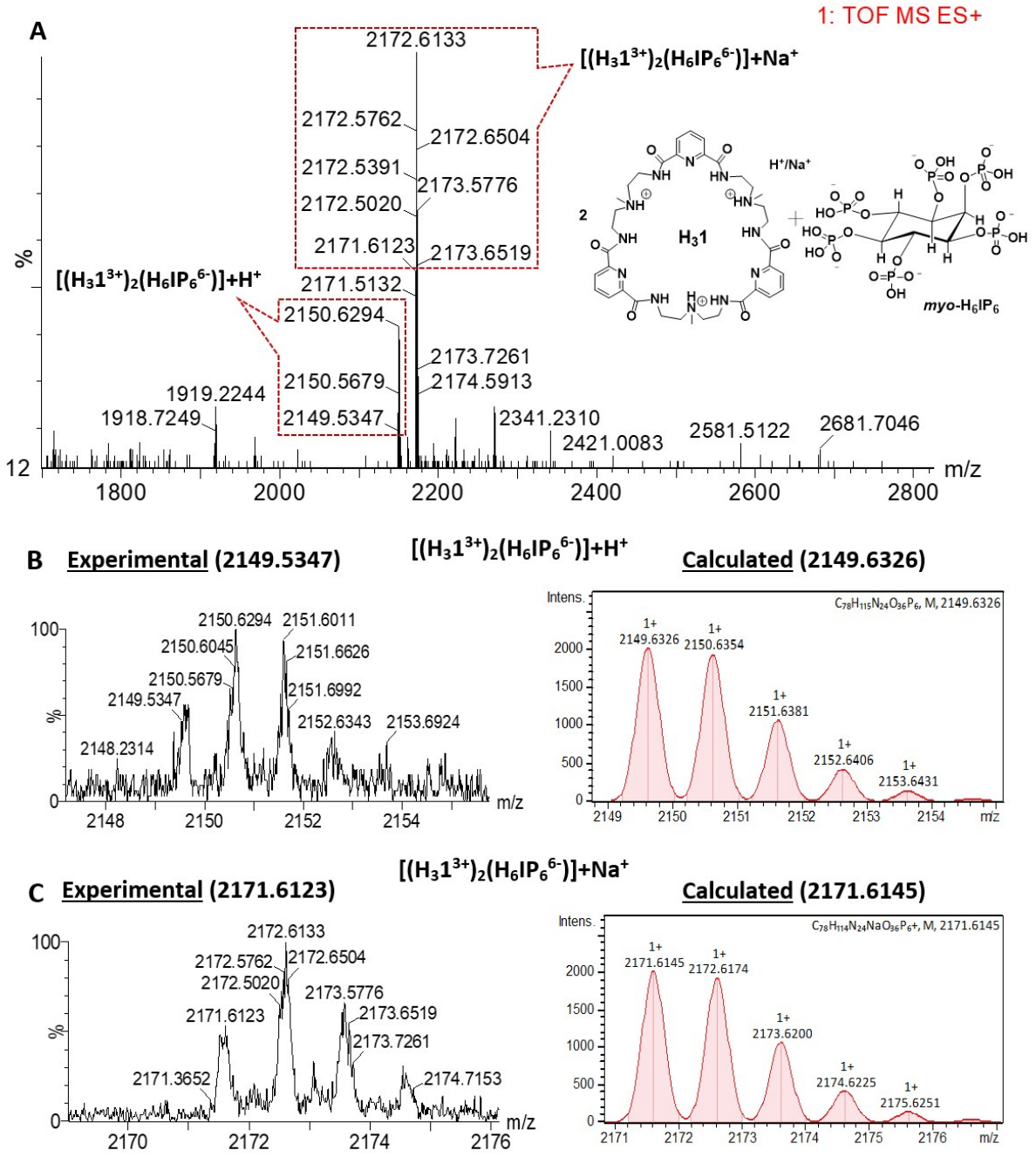

Fig. S15. (A) ESI-MS spectrum of redissolved crystals show the appearance of parent peaks corresponding to the formation of the macrocyclic-$H_6IP_6^{6-}$ sandwich complexes $[(H_3\mathbf{1}^{3+})_2(H_6IP_6^{6-})]$. (**B**) and (**C**) Correlation of two different experimental (left) and calculated (right) peaks (complex + H^+ and complex + Na^+) of the ESI-MS spectrum of the complex, respectively.

S5 DOSY Analysis

DOSY diffusion experiment to determine solution structure

DOSY NMRs were recorded on a Bruker Avance AVIII 600 MHz NMR at 298 K with water suppression. All NMR data were analyzed using MestreLab Mnova software. For DOSY NMR analysis of sandwich complex, sample was prepared by mixing **1**: $[K^+]_2[H_{10}IP_6^{2-}]$ in 2:1 ratio (10 mM, pH 5.87). Sample volumes were 500 µL and the concentration of all samples were 10 mM in DMSO-d_6:D_2O (1:1). The NMR spectra of $[K^+]_2[H_{10}IP_6^{2-}]$ (pH 1.68) were recorded in D_2O. Diffusion coefficients and hydrodynamic radii are correlated theoretically by the Stokes-Einstein relation:

$r_s = kT/(6\pi\eta D)$ where

D is the diffusion coefficient,

k is the Boltzmann constant (1.38×10^{-23} $m^2Kgs^{-2}K^{-1}$),

T is the temperature in Kelvin (298K),

η is the viscosity of the solution,

η (D_2O) = 1.10×10^{-3} $kgm^{-1}s^{-1}$,[S1] η (DMSO-d_6:D_2O, 1:1) = 2.83×10^{-3} $kgm^{-1}s^{-1}$,[S2]

r_s is the hydrodynamic radius of molecular sphere,

$2\times r_s$ is the hydrodynamic diameter.

Table S1. DOSY results for solution sizes of *myo*-IP_6^{n-}, macrocycle **1**, and **2**, $[(H_3\mathbf{1}^{3+})_2(myo\text{-}IP_6^{6-})]$.

Samples	Diffusion D ($\times10^{-6}$ cm^2s^{-1})	Diffusion D ($\times10^{-10}$ m^2s^{-1})	r_s ($\times10^{-10}$ m)	DOSY Diameter (Å)	Crystal Diameter (Å)
***myo*-IP_6^{n-} (1a5e)**	Average: [(4.79±0.2) + (3.32±0.2)]/2 = 4.05±0.2	4.05±0.2	4.90	9.8	10.3 (*myo*-IP_6^{6-}) 10.3 (*myo*-IP_6^{3-})[10]
1	1.01±0.1	1.01±0.1	7.64	15.3	16.0
2	0.71±0.09	0.71±0.09	10.86	21.7	22.3

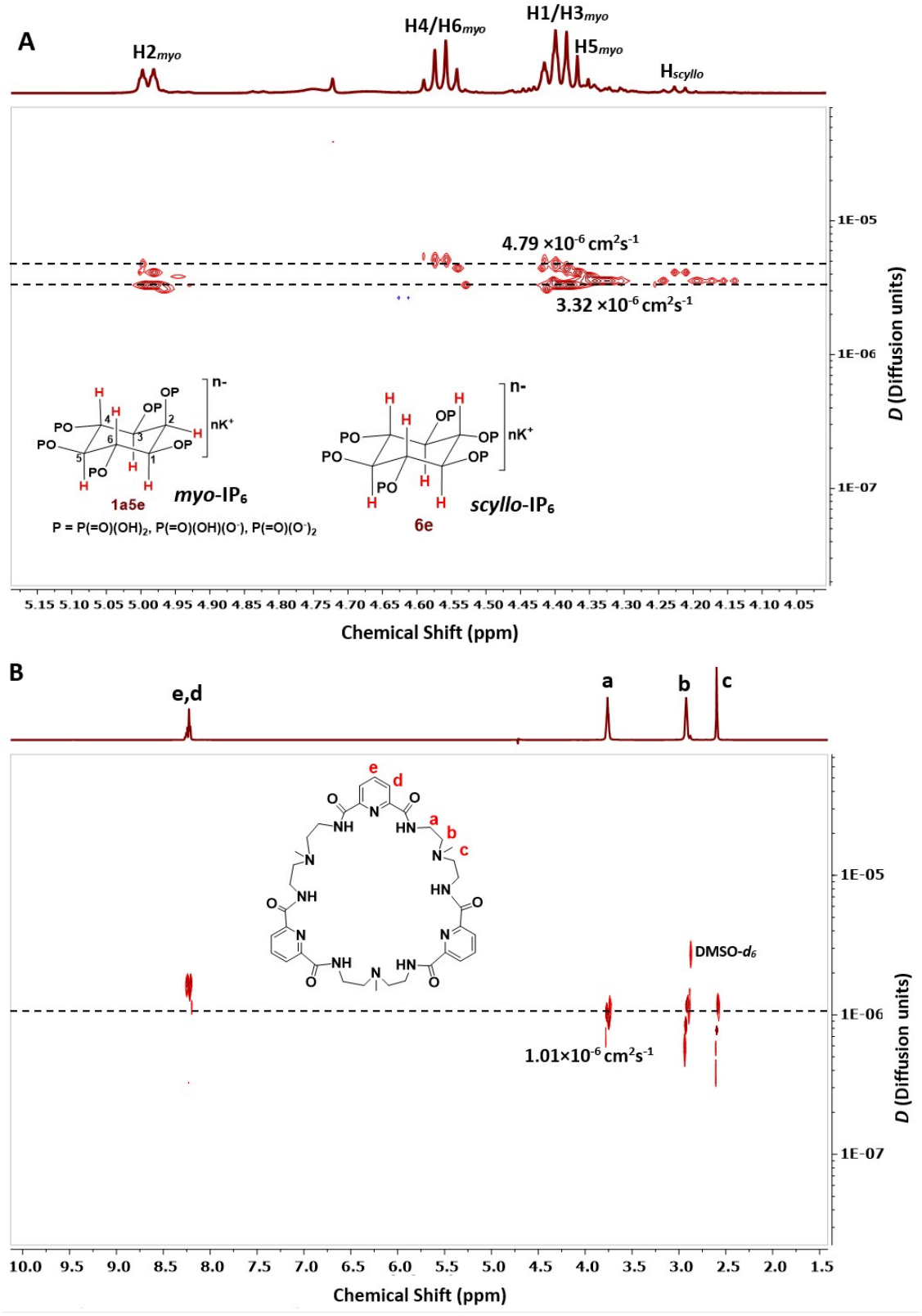

Fig. S16. 2D DOSY NMR spectra of **(A)** $[K^+]_2[H_{10}IP_6^{2-}]$ from Sigma-Aldrich in D_2O and **(B)** macrocycle **1** in DMSO-d_6:D_2O (1:1); the units of *D* are cm^2s^{-1}.

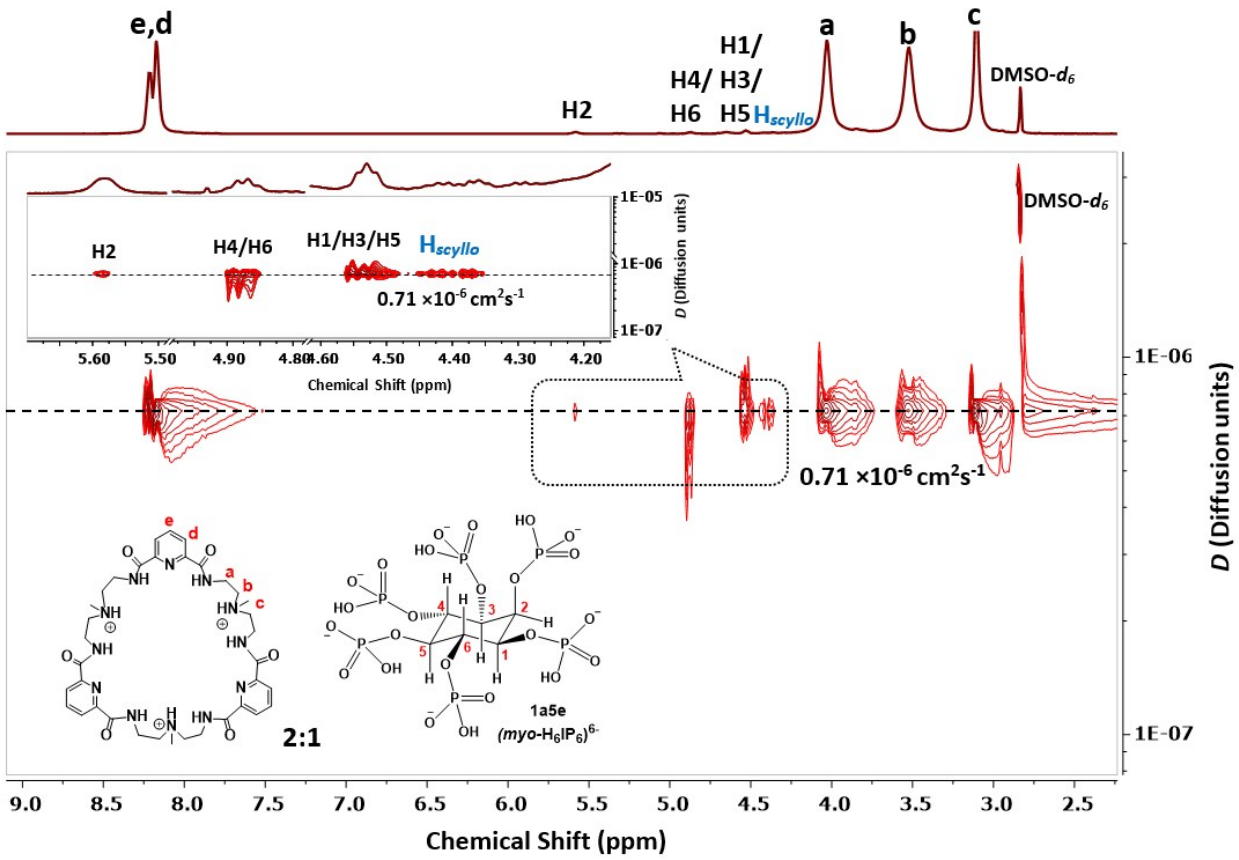

Fig. S17. 2D DOSY NMR spectra of $[(H_3\mathbf{1}^{3+})_2(H_6IP_6^{6-})]$ sandwich complex in DMSO-d_6:D_2O (1:1); inset showing the expanded 2D-spectrum of encapsulated inositol phosphates. The units of D are cm^2s^{-1}.

S6 X-ray Crystallographic Studies

Data Collection and Structure Solution for $1\cdot4H_2O$, $2\cdot36.6H_2O\cdot CH_3OH$ and $3\cdot25.7H_2O\cdot2CH_3CN$

Complete sets of unique reflections were collected with monochromated CuKα radiation for single-domain crystals of all three compounds. Totals of 3847 (**1**), 2843 (**2**) and 829 (**3**) 1.0°-wide ω- or ϕ-scan frames with counting times of 4-6 seconds (**1**) or 12-60 seconds (**2** and **3**) were collected on a Platinum 135 CCD area detector. X-rays were provided by a high-flux Bruker MicroStar microfocus rotating anode operating at 45kV and 60 mA and equipped with Helios high-brilliance multilayer x-ray optics. Preliminary lattice constants were obtained with the Bruker program SMART.[S3] Integrated reflection intensities for all three compounds were produced using the Bruker program SAINT.[S4] Each data set was corrected empirically for variable absorption effects using equivalent reflections. The Bruker software package SHELXTL was used to solve each structure using "direct methods" techniques. All stages of weighted full-matrix least-squares refinement were conducted using Fo^2 data with the SHELXTL v2014.11-0 software package.[S5] The relevant crystallographic and structure refinement data for all three structures compounds are given in Table S2.

The final structural model for each structure incorporated anisotropic thermal parameters for all nonhydrogen atoms and isotropic thermal parameters for all included hydrogen atoms. The macrocycles in all three crystals were ordered. All hydrogen atoms in **1** were located in a difference Fourier and incorporated into the structural model with isotropic thermal parameters that were allowed to vary in least-squares refinement cycles.

The macrocycle and *myo* and *scyllo*-IP_6 hydrogen atoms in **2** and **3**, respectively (except the hydroxyl hydrogen in on O24 in **2**) were fixed at idealized riding model sp^2- or sp^3-hybridized positions with C-H bond lengths of 0.95 – 1.00 Å, N-H bond lengths of 0.88 Å or 1.00 Å and O-H bond lengths of 0.84Å. The macrocylic methyl of **3** was refined as an idealized rigid rotor (with a C-H bond length of 0.98 Å) that was allowed to rotate freely about its N-C bond in least-squares refinement cycles. All methyl groups in **2** were incorporated into the structural model as fixed sp^3-hybridized riding-model rigid groups with C-H bond lengths of 0.98 Å and idealized staggered geometry.

Protonation sites for *myo* and *scyllo*-IP_6 phosphates were chosen based on short intramolecular O---O contacts and significantly elongated P-O bonds. All of the phytate O-H hydrogens except the one on O24 in **2** (which was refined as an individual isotropic atom) were incorporated in the structural model as idealized sp^3-hybridized rigid rotors that were allowed to rotate freely about their P-O bonds in least-squares cycles. Hydrogen atoms on water molecules of crystallization in **2** were fixed wherever possible at idealized positions based on hydrogen bonding considerations. Hydrogen atoms were only placed on waters in **2** when their placement was unambiguous. While all of the water molecules of crystallization in **1** are ordered and present at full-occupancy, many of the lattice sites for water molecules of crystallization in **2** and all but one of those in **3** are only partially occupied.

The asymmetric unit of **2** has 27 full-occupancy sites (O1W to O27W), 19 half occupancy sites (O28W to O46W) and 2 sites (O47W and O48W) with an occupancy factor of 0.30. The oxygen atom for the methanol solvent molecule of crystallization in **2** is also 50/50 disordered between two sites.

The asymmetric unit of **3** has one full-occupancy site, O1W(0.33/0.33) and six disordered, partial-occupancy water molecules of crystallization: O2W(0.80/1.00), O3W(0.70/1.00), O4W(0.40/1.00) O5W(0.50/1.00), O6W(0.20/0.33). Water molecule O7W in **3** is disordered over three sites in the asymmetric unit: O7W(0.50), O7W"(0.30) and O7W'(0.20).

The crystal of **1** diffracted very well and gave a highly-precise structure. But the crystals of **2** and **3** with disordered water molecules of crystallization diffracted quite poorly even though both used 60-second data frames and a high-flux x-ray source for the high-angle data. Even with the much longer-than-usual counting times, the mean I/σ(I) ratio was less than 3.00 for data beyond 0.96 Å resolution for **2** and 1.02 Å resolution for **3**. Nonetheless, diffracted intensities to 0.87 Å for **2** and **3** were collected, integrated and

included in least-squares refinement cycles. Inclusion of this very weak high-angle data is obviously responsible for the higher (0.119 and 0.158) R_1 values for **2** and **3**, respectively.

Mild restraints were applied to the anisotropic thermal parameters of the following partial-occupancy water molecules: O39W, O45W and O48W in **2**; and O5W, O7W' and O7W" in **3**.

CCDC: 1947225 (**1**·4H_2O),
1947224 (**2**·36.6H_2O·CH_3OH) and
1947283 (**3**·25.7H_2O·2CH_3CN)

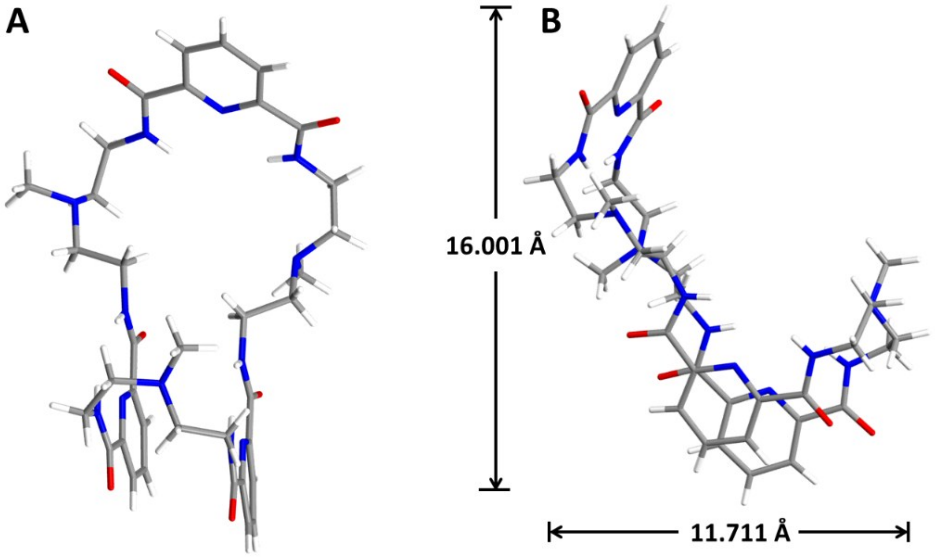

Fig. S18. Perspective views **(A)** and **(B)** of the free base macrocycle **1** with dimensions (Å) (H_2O not shown for clarity).

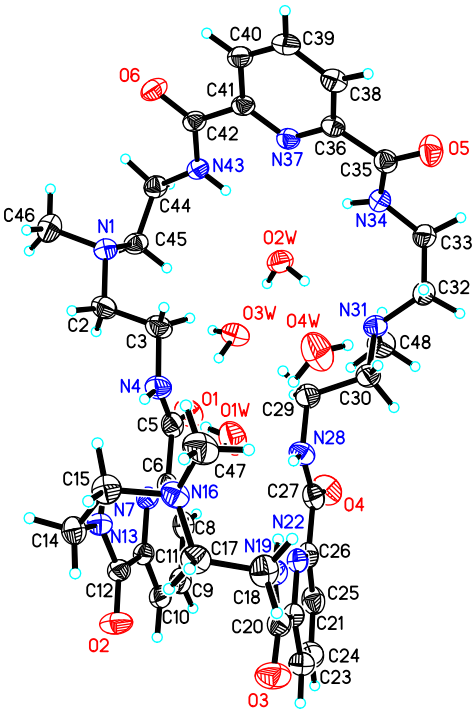

Fig. S19. Thermal ellipsoid depiction of macrocycle **1**·4H_2O at 50% probability.

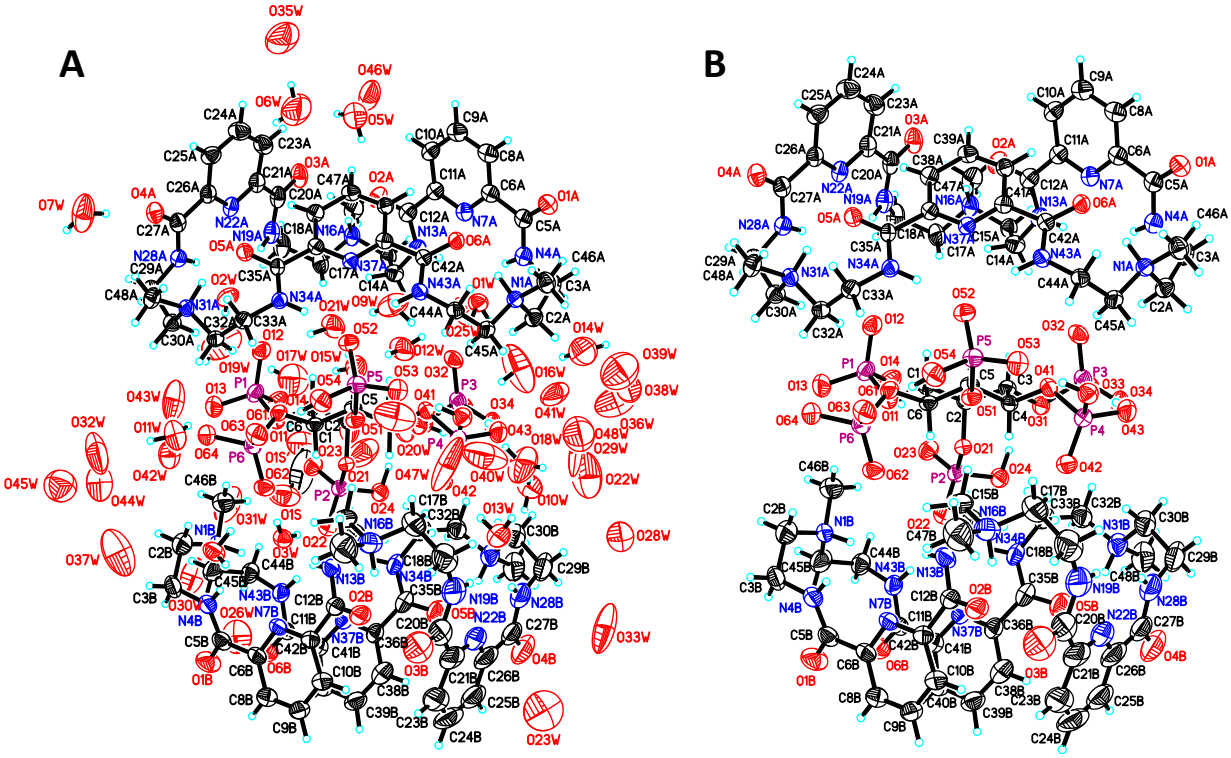

Fig. S20. Thermal ellipsoid depiction of phytate complex **2**·36.6H_2O·CH_3OH at 30% probability: **(A)** with and **(B)** without solvent molecules.

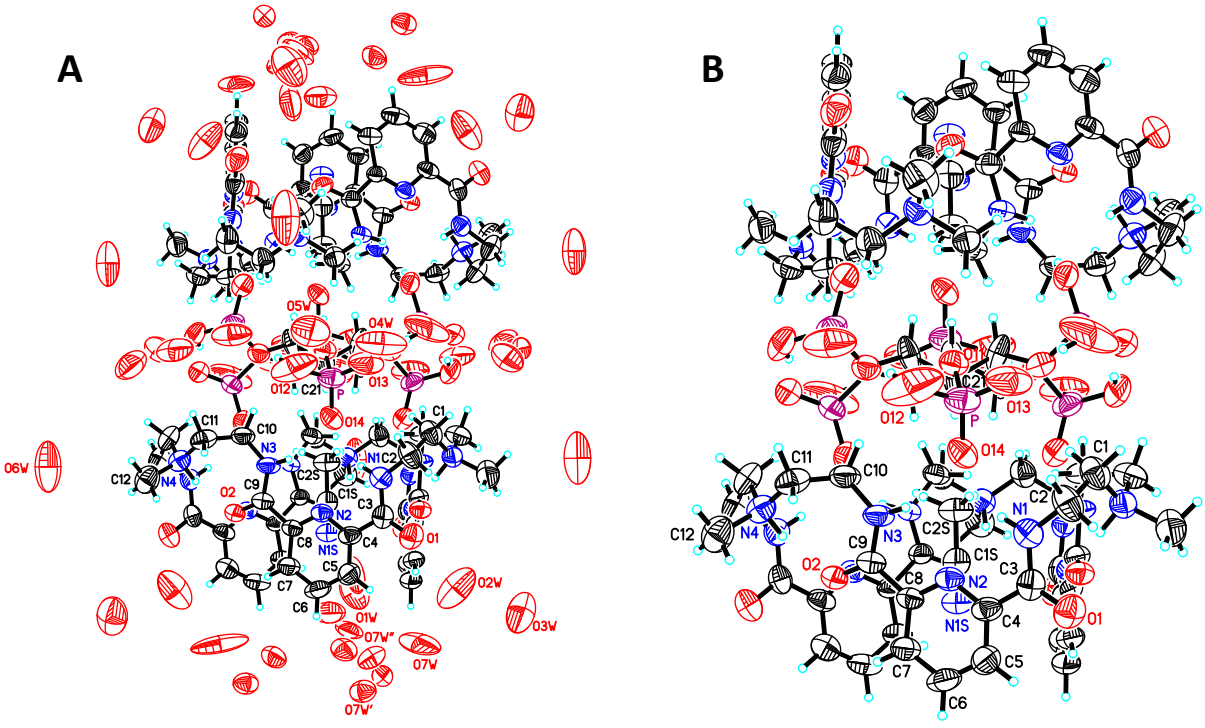

Fig. S21. Thermal ellipsoid depiction of *scyllo*-IP_6 complex **3**·25.7H_2O·2CH_3CN at 30% probability: **(A)** with and **(B)** without solvent molecules.

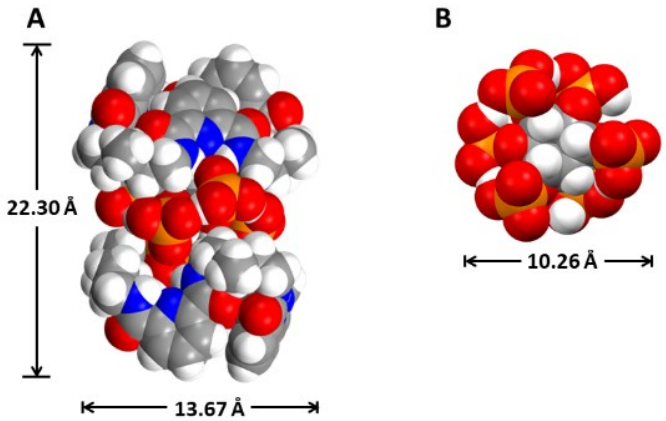

Fig. S22. Dimensions of the *myo*-IP_6 complex and the *myo*-IP_6 ion from the crystal structure.

Table S2. Crystal Data and Structure Refinement for **1**·$4H_2O$, **2**·$36.6H_2O$·CH_3OH, and **3**·$25.7H_2O$·$2CH_3CN$.

	1·$4H_2O$	**2**·$36.6H_2O$·CH_3OH	**3**·$25.7H_2O$·$2CH_3CN$
Empirical formula	$C_{36}H_{56}N_{12}O_{10}$	$C_{79}H_{191.20}N_{24}O_{74.10}P_6$	$C_{82}H_{171.40}N_{26}O_{59.60}P_6$
Formula weight	816.92	2849.17	2661.26
Temperature	200(2) K	200(2) K	200(2) K
Wavelength	1.54178 Å	1.54178 Å	1.54178 Å
Crystal system	Triclinic	Monoclinic	Trigonal
Space group	$P\bar{1}$ – C_i^1 (No. 2)	C2/c – C_{2h}^6 (No. 15)	R-3 – C_{3i}^2 (No. 148)
a	10.6732(6) Å	49.267(4) Å	18.3819(8) Å
b	12.9990(8) Å	14.9082(12) Å	18.3819(8) Å
c	16.3255(10) Å	39.726(3) Å	35.5789(18) Å
a	75.5241(12)°	90°	90°
β	85.8338(13)°	100.616(4)°	90°
γ	71.3608(13)°	90°	120°
Volume	2078.0(2) $Å^3$	28679(4) $Å^3$	10411.3(10) $Å^3$
Z	2	8	3
Density (calculated)	1.306 g/cm^3	1.320 g/cm^3	1.273 g/cm^3
Absorption coefficient	0.807 mm^{-1}	1.595 mm^{-1}	1.538 mm^{-1}
F(000)	872	12128	4237
Crystal size	0.10 x 0.20 x 0.22 mm^3	0.08 x 0.13 x 0.25 mm^3	0.08 x 0.09 x 0.18 mm^3
Number of data frames/time	3847/4-6 seconds	2843/12-60 seconds	829/15-60 seconds
Theta range	2.80 to 68.20°	2.63 to 63.69°	3.73 to 62.63°
Index ranges	-10≤h≤12, -14≤k≤15, -	-56≤h≤52, -16≤k≤13, -	-17≤h≤20, -20≤k≤17, -

	19≤l≤18	46≤l≤44	40≤l≤31
Reflections collected	27929	77727	12128
Independent reflections	7252 [R_{int} = 0.037]	22167 [R_{int} = 0.070]	3641 [R_{int} = 0.072]
Completeness/θ_{max}	97.8%/66.00°	96.1%/62.20°	98.0%/62.63°
Absorption correction	Multi-scan	Multi-scan	Multi-scan
Max. and min. transmission	1.000 and 0.828	1.000 and 0776	1.000 and 0.711
Refinement method	Full-matrix least-squares on F^2	Full-matrix least-squares on F^2	Full-matrix least-squares on F^2
Data / restraints / parameters	7252 / 0 / 748	22167 18 / 1761	3641 / 18 / 297
Goodness-of-fit on F^2	1.021	1.054	1.064
Final R indices [I>2σ(I)]	R_1 = 0.035, wR_2 = 0.093	R_1 = 0.119, wR_2 = 0.324	R_1 = 0.158, wR_2 = 0.351
R indices (all data)	R_1 = 0.037, wR_2 = 0.094	R_1 = 0.160, wR_2 = 0.366	R_1 = 0.219, wR_2 = 0.392
Largest diff. peak and hole	0.38 and -0.18 $e^-/Å^3$	1.06 and -0.60 $e^-/Å^3$	0.93 and -0.34 $e^-/Å^3$

S7 References

S1. A. M. Schradera, Jr. S. H. Donaldson, J. Son, C.-Y. Cheng, D. W. Lee, S. Hana and J. N. Israelachvili, *Proc. Natl. Acad. Sci. U. S. A.*, 2015, **112**, 10708.

S2. R. G. LeBel and D. A. I. Goring, *J. Chem. Eng. Data*, 1962, **7**, 100.

S3. Data Collection: SMART Software in APEX2 v2014.11-0 Suite. Bruker-AXS, 5465 E. Cheryl Parkway, Madison, WI 53711-5373 USA.

S4. Data Reduction: SAINT Software in APEX2 v2014.11-0 Suite. Bruker-AXS, 5465 E. Cheryl Parkway, Madison, WI 53711-5373 USA.

S5. Refinement: SHELXTL Software in APEX2 v2014.11-0 Suite. Bruker-AXS, 5465 E. Cheryl Parkway, Madison, WI 53711-5373 USA.